ACS APPLIED MATERIALS & INTERFACES

Research Article

www.acsami.org

Vanadium Oxychloride/Magnesium Electrode Systems for Chloride Ion Batteries

Ping Gao,[†] Xiangyu Zhao,*[,‡,§] Zhirong Zhao-Karger,[§] Thomas Diemant,[∥] R. Jürgen Behm,[†,∥] and Maximilian Fichtner*[,†,§]

[†]Helmholtz-Institute Ulm for Electrochemical Energy Storage (HIU), Helmholtzstrasse 11, 89081 Ulm, Germany

[‡]College of Materials Science and Engineering, Nanjing Tech University, 5 Xinmofan Road, 210009 Nanjing, China

[§]Institute of Nanotechnology, Karlsruhe Institute of Technology (KIT), Hermann-von-Helmholtz-Platz 1, 76344 Eggenstein-Leopoldshafen, Germany

[∥]Institute of Surface Chemistry and Catalysis, Ulm University, Albert-Einstein-Allee 47, 89081 Ulm, Germany

Supporting Information

ABSTRACT: We report a new type of rechargeable chloride ion battery using vanadium oxychloride (VOCl) as cathode and magnesium or magnesium/magnesium chloride ($MgCl_2$/Mg) as anode, with an emphasis on the VOCl-$MgCl_2$/Mg full battery. The charge and discharge mechanism of the VOCl cathode has been investigated by X-ray diffraction, X-ray photoelectron spectroscopy, and electrochemical measurements, demonstrating the chloride ion transfer during cycling. The VOCl cathode can deliver a reversible capacity of 101 mAh g^{-1} at a current density of 10 mA g^{-1} and a capacity of 60 mAh g^{-1} was retained after 53 cycles in this first study.

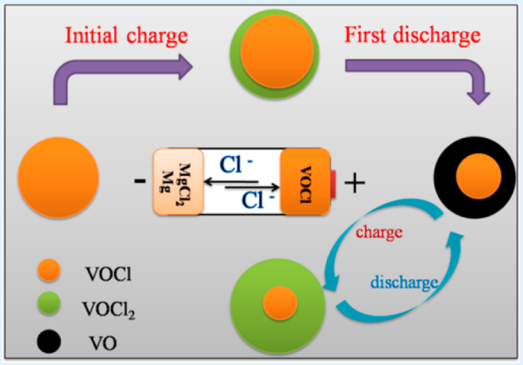

KEYWORDS: *chloride ion, vanadium oxychloride, rechargeable battery, magnesium anode, electrochemistry*

1. INTRODUCTION

Secondary batteries based on a cation shuttle such as Li^+, Na^+, Mg^{2+}, Zn^{2+}, and Al^{3+} have been demonstrated in recent years.[1−10] Although many achievements have been obtained for consumer electronics, electric vehicles, transportation, and military with these batteries, it remains a challenge to develop a high energy density, safe, cheap, and environment-friendly energy storage device. In this respect, an alternative rechargeable battery based on an anion shuttle, such as fluoride ion battery or chloride ion battery, could possibly meet such requirements as several electrons can be transferred during the electrochemical reaction, leading to a high theoretical energy density.[11−14] Moreover, using lithium-free anode materials including magnesium, calcium, and others could provide an alternative way to develop a low cost and safe rechargeable device for electrochemical energy storage.

The chloride ion battery is a rechargeable battery based on chloride ion transfer. It uses a liquid electrolyte at room temperature and offers a broad variety of high potential electrochemical couples and high theoretical volumetric energy density.[13,14] The overall cathodic and anodic electrochemical reactions are as follows

$$\text{at cathode: } MClx + xe^- \leftrightarrow M + xCl^-$$

$$\text{at anode: } M' + xCl^- \leftrightarrow M'Clx + xe^-$$

$MClx$ can be a transition metal chloride (e.g., $BiCl_3$, $CuCl_2$, VCl_3, or $FeCl_3$) or a transition metal oxychloride (e.g., FeOCl or BiOCl), M′ is a metal anode (e.g., Li, Na, Mg, Ca, or Ce). The first concept of chloride ion battery was demonstrated by using an ionic liquid electrolyte (IL), a lithium foil anode, and $CoCl_2$, VCl_3, or $BiCl_3$ as cathode. These cathodes showed initial reversible discharge capacities of 105, 111, and 176 mAh g^{-1}, respectively.[13] In this battery system, a challenge is to suppress the dissolution of the involved metal chlorides in the liquid electrolyte. Metal oxychloride compounds such as FeOCl and BiOCl have been proposed as potential cathode materials due to their higher stability in ILs and better cycling behavior.[14]

Herein, we report a new rechargeable chloride ion battery using vanadium oxychloride (VOCl) as cathode and a lithium-free anode composed of a $MgCl_2$/Mg composite. In this battery, the VOCl electrode is stable in the liquid electrolyte and could be oxidized to vanadium oxydichloride ($VOCl_2$) during charging, which has a high theoretical capacity of 388 mAh g^{-1} based on the reaction of VO/$VOCl_2$. Moreover, a large Gibbs free energy generated between $VOCl_2$ and Mg would yield a high electromotive force (EMF) of 1.86 V.

Received: September 19, 2014
Accepted: November 24, 2014
Published: November 24, 2014

dx.doi.org/10.1021/am5064266 | ACS Appl. Mater. Interfaces 2014, 6, 22430−22435

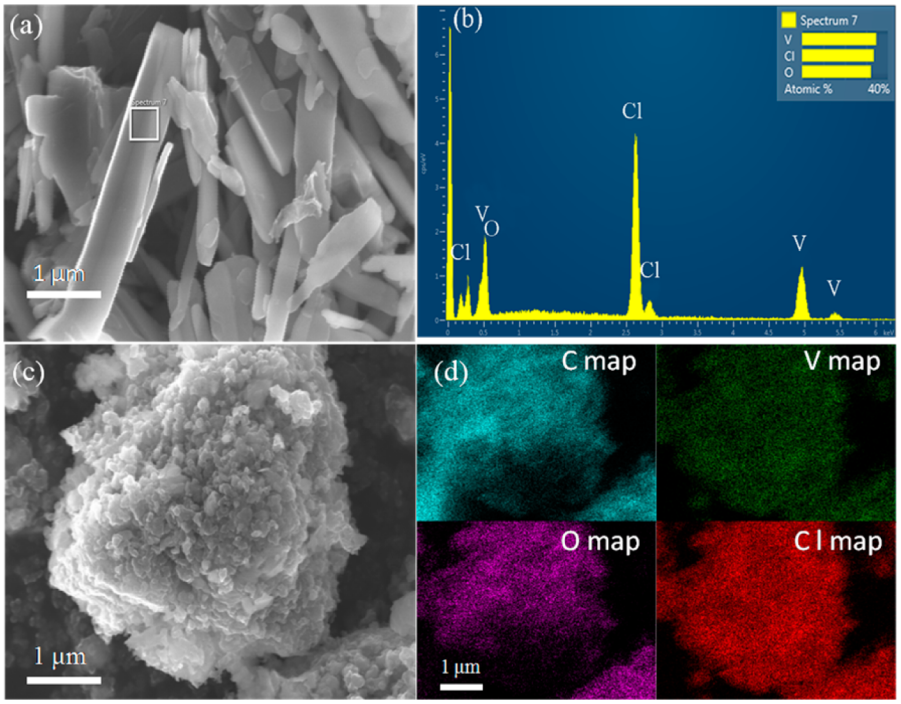

Figure 1. (a) SEM image of the as-prepared VOCl and (b) corresponding EDX spectrum from the marked area in a. (c) SEM image of the as-prepared VOCl/C and (d) corresponding elemental mapping of carbon, vanadium, oxygen, and chlorine.

Furthermore, magnesium has a theoretical specific volumetric capacity of 3833 mAh cm^{-3}, which is much higher than 2046 mAh cm^{-3} of lithium.

2. EXPERIMENTAL SECTION

VOCl was prepared by a solid−gas reaction.[15] A mixture of V_2O_3 (98%, Sigma-Aldrich) and VCl_3 (97%, Sigma-Aldrich) with a molar ratio of 1:1.8 was loaded in an evacuated and sealed quartz tube, and then it is kept at a temperature of 893 K for 120 h with a heating rate of 1 K min^{-1}. The obtained brown VOCl material was washed with dimethylformamide, ethanol, and petroleum ether to remove residual VCl_3. The VOCl/C cathode material was prepared by ball milling a mixture of 80 mass % VOCl and 20 mass % carbon black (Sigma-Aldrich) using a silicon nitride vial and balls for 1 h at a speed of 200 rpm under an argon atmosphere. The $MgCl_2$/Mg/C composite material was prepared by ball-milling anhydrous $MgCl_2$ (98%, Sigma-Aldrich, 50 mass %), Mg powder (99.8%, Alfar Aesar, 40 mass %), and carbon black (10 mass %) using a tungsten carbide vial and tungsten carbide balls for 10 h at 300 rpm. A similar procedure was applied for preparing the Mg/C composite material with 20 mass % carbon black. Anhydrous ionic liquids of 1-butyl-1-methylpiperidinium bis-(trifluoromethylsulfonyl)imide (PP_{14}TFSI, 99%, IoLiTech) and 1-butyl-1-methylpiperidinium chloride (PP_{14}Cl, 99%, IoLiTech) were dried at 358 K for 72 h under a vacuum.

The cathode electrodes were prepared by grinding a mixture of active material (VOCl/C, 80 mass %), poly(vinylidene difluoride) binder (PVDF, 10 mass %) and carbon black (10 mass %) with *N*-methylpyrrolidone (NMP) as solvent for 30 min in a mortar. The obtained slurry was then spread on a stainless steel foil with 12 mm in diameter and dried overnight at 353 K under a vacuum. The mass loading of the cathode electrode was 1.0−1.5 mg per piece. The anode electrode was prepared by pressing the composite into a pellet with 20 mg in mass and 11 mm in diameter.

Electrochemical tests were conducted using Swagelok-type cells. The cells were assembled in an argon-filled glovebox by using VOCl/C as cathode, glass fiber filter (GF/D, Whatman) as separator, and $MgCl_2$/Mg/C or Mg/C as anode. A mixture of 0.5 M PP_{14}Cl in PP_{14}TFSI was used as electrolyte. Charge and discharge measurements were performed in a voltage window of 2.5−0.6 or 2.2−0.6 V at a current density of 5 or 10 mA g^{-1}, using an Arbin BT2000 battery system at 298 K. The cyclic voltammetry (CV) and electrochemical impedance spectroscopy (EIS) data were collected using a Biologic VMP-3 electrochemical workstation. The sweep rate of CV was 0.05 mV s^{-1} in the potential range of 2.5−0.6 V. The frequency range of EIS was from 200 kHz to 100 mHz with an ac amplitude of 10 mV.

Powder X-ray diffraction patterns were obtained on a Philips X'PERT diffractometer equipped with Cu Kα radiation source (operated at 40 kV, 40 mA). Scanning electron microscope (SEM) and energy-dispersive X-ray spectroscopy (EDX) were carried out using a ZEISS LEO 1530 instrument. X-ray photoelectron spectroscopy (XPS) data was recorded on a physical electronics PHI 5800 ESCA system using monochromatized Al Kα radiation (13 kV, 250 W) and a pass energy of 29.35 eV for the detail scan in the V (2p) binding energy (BE) region. For BE calibration, the main C_{1s} peak was set to 284.8 eV.

3. RESULTS AND DISCUSSION

Powder X-ray diffraction (XRD) patterns of as-prepared VOCl and VOCl/C materials are shown in Figure S1 (Supporting Information). All reflections can be indexed and assigned to the orthorhombic VOCl phase with the space group of *Pmmn* (PDF card no. 01-085-0353) except for few impurities in the ball milled VOCl/C composite.[16] The morphology and size of the as-prepared VOCl and VOCl/C materials are shown in Figure 1 and Figure S2. The as-prepared VOCl material consists of rodlike particles with a size of around 100−500 nm in width and about 2 μm in length (Figure 1a and Figure S2a and b). The EDX spectrum in Figure 1b shows that the atomic ratio of vanadium, oxygen, and chlorine in the as-prepared VOCl material is close to the theoretical value of 1:1:1. The EDX elemental mapping of the as-prepared VOCl indicates a uniform elemental distribution, as shown in Figure S3. Particles with a diameter of 100−500 nm were obtained after ball milling of the VOCl/C composite (Figure 1c and Figure S2c and d). The EDX elemental mapping of vanadium, oxygen, chlorine, and carbon in the VOCl/C composite also demonstrates a

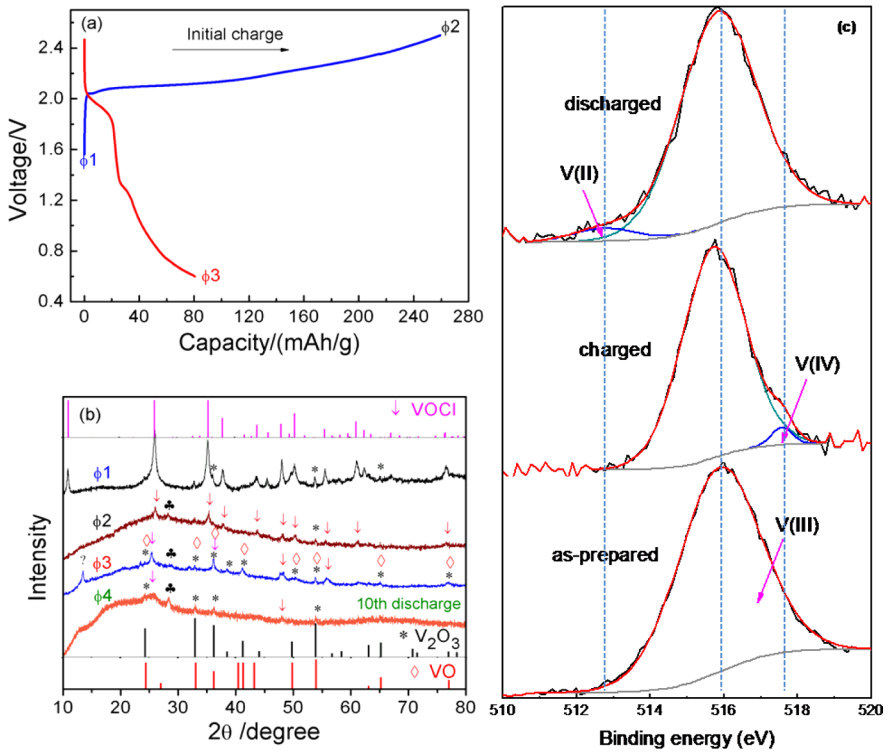

Figure 2. (a) Initial charge and discharge profiles of VOCl-MMC, (b) powder XRD patterns, and (c) $V_{2p3/2}$ XPS spectra of the VOCl/C electrode at different states.

uniform elemental distribution, as shown in Figure 1d. The well-distributed carbon black is necessary for the electrical transport in the VOCl/C composite.

In order to understand the electrochemical reactions of the electrodes, the batteries were disassembled at various charge and discharge states and the cathodes were analyzed by ex-situ XRD and XPS, as shown in Figure 2. The chloride ion battery using VOCl/C as cathode and $MgCl_2$/Mg/C as anode is denoted as VOCl-MMC. Figure 2a exhibits the initial charge and discharge curves of VOCl-MMC within a potential window of 2.5−0.6 V at a current density of 5 mA g^{-1}. Two plateaus at 1.9 and 1.3 V were observed in the first discharge process.

Ex-situ XRD in Figure 2b shows the phase composition of the VOCl/C cathode at different states during the first cycle and after 10 cycles. For the as-prepared VOCl/C material, main reflections can be indexed and assigned to the orthorhombic VOCl phase. A small amount of V_2O_3 was observed, however (Figure 2b line ϕ1). This may be caused by partial decomposition of VOCl during ball milling. When the VOCl/C electrode was charged to 2.5 V (Figure 2b line ϕ2), the peak intensity of the VOCl phase decreased drastically. Nevertheless, the $VOCl_2$ phase, which is supposed to be formed by electrochemical oxidation of VOCl, was not detected which could be due to the formation of nanosized and/or amorphous phase. Upon discharging the electrode to 0.6 V at the first cycle (Figure 2b line ϕ3), the diffraction peaks related to VO phase (PDF card no. 00-038-0974), V_2O_3 phase (PDF card no. 34-0187), and the VOCl phase were observed. One diffraction peak at 13.5° was not identified. The formation of VO phase demonstrates that the V^{3+} is reduced to V^{2+} and chloride ions dissociate from the VOCl during discharge. For the VOCl/C electrode at the discharged state after 10 cycles, the dominant phase of V_2O_3 with contributions of VOCl was detected, whereas VO was not detected.

It should be mentioned that the conclusions in this paper could not be drawn on the basis of XRD data alone, as there were sometimes difficulties in detecting phases, possibly due to their nanoscale size or for reasons which are described below. Hence, additional methods such as XPS were applied, in particular to detect oxidation states of the vanadium in the different stages of charge and discharge.

Conversion reactions may refine the particles and lead to the formation of large fresh and active surfaces, an effect which has been observed for a number of conversion materials. Then the VO with higher activity was formed after 10 cycles. However, VO of the discharged product was gradually oxidized to V_2O_3 during a long time (about 5 h) XRD measurement, although a protected XRD holder assembled in the glovebox was used. A diffraction peak was detected at 28.4° in the 10th discharge state and its intensity increased as compared to that of the electrodes (see lines ϕ2 and ϕ3 in Figure 2b) during the first cycle. This may be related to the formation of VO_2 phase (PDF no. 43-1051, Figure S4), which was formed by the oxidation of vanadium oxide with lower vanadium valence during XRD measurement.

XPS measurements were carried out to get a further insight on the oxidation state of vanadium during cycling. The XPS survey spectra and the $V_{2p3/2}$ core level spectra of the VOCl/C electrode in the as-prepared, charged to 2.5 V and discharged to 0.6 V states are shown in Figure S5 and Figure 2 c, respectively. The binding energy of $V_{2p3/2}$ corresponding to the as-prepared VOCl/C electrode was located at 515.7 eV, which is consistent with V^{3+} oxidation state.[17,18] When the VOCl/C electrode was charged to 2.5 V, $V_{2p3/2}$ peaks at 515.7 and 517.6 eV were observed, which can be assigned to the vanadium oxidation states of V^{3+} (VOCl) and V^{4+} ($VOCl_2$), respectively.[19] It was found that the intensity of the peak at 517.6 eV corresponding to V^{4+} species was lower than that of the main peak at 515.7 eV.

dx.doi.org/10.1021/am5064266 | ACS Appl. Mater. Interfaces 2014, 6, 22430−22435

This low intensity peak could be due to the partial electrochemical oxidation of VOCl to $VOCl_2$ in the first charge process. For the discharged electrode, the $V_{2p3/2}$ peak located at 512.7 eV was related to the VO phase[17] and the peak at 515.8 eV was assigned to the V^{3+} species, which can be attributed to the unreacted VOCl in the discharge process. This is consistent with and complements the XRD result in Figure 2b.

Figure 3 shows the cyclic voltammetry (CV) curves of the VOCl-MMC electrode system in the potential window of 2.5−0.6 V at the initial five cycles. In the CV measurement, the potential was initially swept from the open circuit voltage (OCV = 1.65 V) to 2.5 V. A broad anodic peak located at 2.4 V was observed in the first scanning from OCV to 2.5 V, which can be assigned to the reaction of $VOCl + Cl^- \rightarrow VOCl_2 + e^-$. Two cathodic peaks appeared in the first cycle at 2.01 and 1.25 V, which could be attributed to the two-step reduction reactions of $VOCl_2 + e^- \rightarrow VOCl + Cl^-$ (EMF = 2.24 V) and $VOCl + e^- \rightarrow VO + Cl^-$ (EMF = 1.49 V), respectively. In the second scan, the anodic peak shifted to a lower potential (~2.35 V) and its intensity decreased. Meanwhile, the intensity of the cathodic peak at around 1.9 V increased upon cycling. This is consistent with the increase of the discharge capacity in the initial cycles, as shown in Figure 4d. A pair of cathodic/anodic peaks at 1.27 and 1.52 V corresponding to the reaction of V^{3+}/V^{2+} was more stable. As mentioned above, two distinct redox couples of 2.35/1.88 and 1.52/1.27 V based on the reactions of chloride ion transfer were observed for the VOCl-MMC electrode system during cycling. The charge and discharge reactions of the VOCl-MMC could be described as

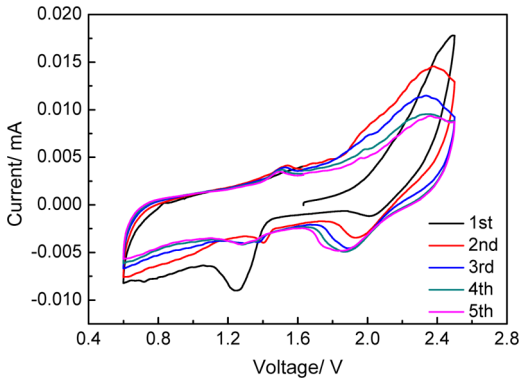

Figure 3. CV curves of the VOCl-MMC electrode system between 2.5 and 0.6 V at a scanning rate of 0.05 mV s^{-1}.

First charge:

$$2VOCl + MgCl_2 \rightarrow 2VOCl_2 + Mg \quad (1)$$

First discharge:

$$2VOCl_2 + Mg \rightarrow 2VOCl + MgCl_2 \quad E = 2.24\ V \quad (2)$$

$$2VOCl + Mg \rightarrow 2VO + MgCl_2 \quad E = 1.49\ V \quad (3)$$

Figure 4a shows the first three charge/discharge curves of the VOCl-Mg full battery using Mg/C as anode in the voltage range of 0.6−2.2 V. The first discharge capacity was 40 mAh g^{-1}, and a plateau at around 1.35 V was observed, which can be ascribed to the reaction $VOCl + e^- \rightarrow VO + Cl^-$. Figure 4b shows the first discharge curves of the batteries using VOCl/C as cathode and two different anodes at 5 mA g^{-1}. The charge and discharge testing of VOCl-MMC was performed between 2.5 and 0.6 V. Two discharge plateaus at 1.95 and 1.3 V for VOCl-MMC and one discharge plateau at 1.35 V for VOCl-Mg

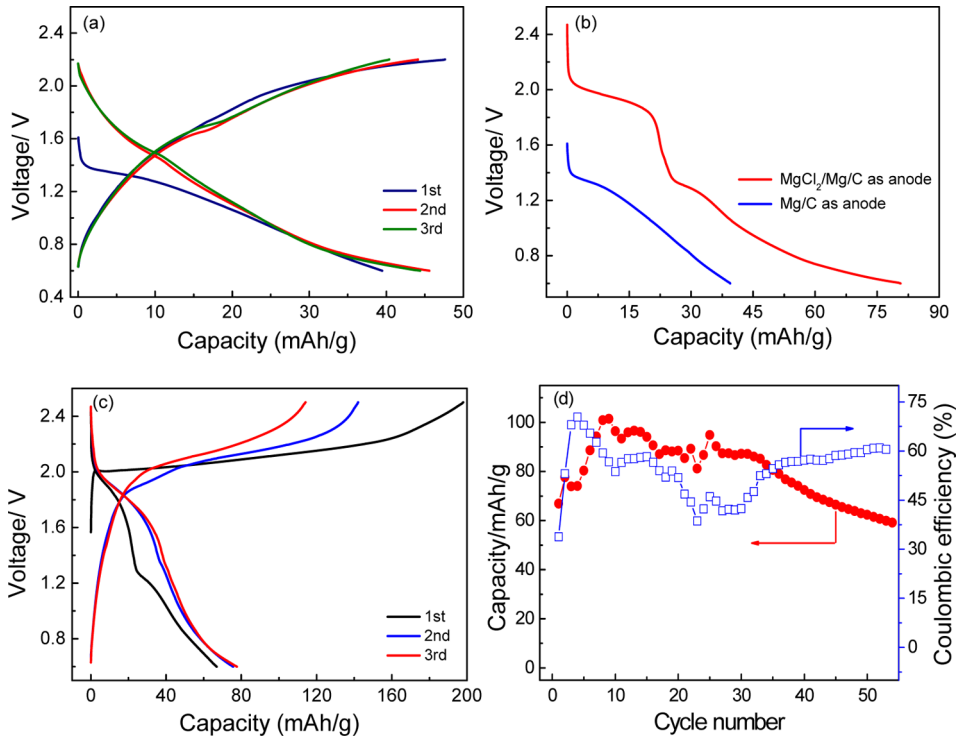

Figure 4. (a) Charge and discharge profiles of the VOCl-Mg full battery at 5 mA g^{-1}. (b) First discharge curves of the full battery using VOCl/C as cathode and Mg/C or $MgCl_2$/Mg/C as anode at 5 mA g^{-1}. (c) Charge and discharge profiles of the VOCl-MMC full battery in the first three cycles at 10 mA g^{-1}. (d) Cycling performance of the VOCl-MMC full battery in 53 cycles.

were observed. The different discharge voltage profiles may be attributed to the different electrochemical reaction processes. In the VOCl-MMC battery, the $VOCl_2$ was obtained after the VOCl electrode was charged to 2.5 V. $VOCl_2$ can provide two chloride ions during the subsequent discharge processes whereas only one chloride ion can be shuttled in the VOCl-Mg battery.

Figure 4c shows the first three cycles of the VOCl-MMC battery at a current density of 10 mA g^{-1}. A first charge capacity of 198 mAh g^{-1} was obtained, and the corresponding discharge capacity of the VOCl/C electrode was 66 mAh g^{-1}. The discharge profile exhibited two plateaus at 1.91 and 1.24 V, which corresponded to the two reduction peaks in the CV patterns (Figure 3). In the second and third cycle, the charge capacity decreased gradually, while the discharge capacity increased with a distinct and higher discharge plateau. This is consistent with the evolution of redox peaks in the CV profiles (Figure 3). The VOCl-MMC battery cycled at a current density of 5 mA g^{-1} showed a similar profile to that of the battery cycled at 10 mA g^{-1} (Figure S6).

Figure 4d shows the cycling performance of the VOCl-MMC battery at a current density of 10 mA g^{-1}. The VOCl/C cathode exhibited an increase in the discharge capacity and also the Coulombic efficiency during the initial several cycles, indicating an activation process, which may be ascribed to the improvement of the electrochemical kinetic performance. It is known that conversion reaction can refine the particle size and thus results in the formation of much more fresh surface for the electrochemical reaction. A maximum discharge capacity of 101 mAh g^{-1} was obtained at the ninth cycle. Then the cathode retained a discharge capacity of 87 mAh g^{-1} in 30 cycles. Subsequently, the capacity decay occurred in the next 20 cycles and the capacity retention was 59% after 53 cycles. In our previous work on BiOCl-Mg and FeOCl-Mg electrode systems, the BiOCl and FeOCl cathodes delivered the first discharge capacities of 102 and 130 mAh g^{-1}, respectively.[20] More than 50% of the theoretical capacity was obtained for both BiOCl and FeOCl cathodes, whereas the maximum discharge capacity of the VOCl cathode was only about 26% of the theoretical capacity. This may be caused by the loss of the electrical contact between the active material and carbon because a large volume change of 292% would occur from $VOCl_2$ to VO during discharge. This value is much larger than that of BiOCl or FeOCl. Similar phenomenon also exists at the anode side. Another possible reason may be related to the sluggish electrochemical kinetic performance of the VOCl-MMC battery system. Electrochemical impedance spectroscopy (EIS) measurement was performed for the VOCl-MMC full battery at different charge and discharge states, as shown in Figure S7. The Nyquist curves are composed of a quasi-semicircle at the high frequency related to the charge transfer process and a straight line at the low frequency correlated to the Warburg impedance (W) by chloride ion diffusion. The simulated results showed that the charge-transfer resistance of the discharged VOCl-MMC was larger than the charged one and it increased after three cycles in the discharged state. This may be related to the sluggish electrochemical kinetics due to the volume change in the cathode and anode. Obviously, only part of the electrode materials were electrochemically active during cycling, leading to a low discharge capacity. The increase of the chloride ion diffusion in both the electrodes and the electrolyte is important for enhancing the electrochemical properties of the VOCl-MMC electrode system in future work.

Based on the electrochemical and structural information above, a first description of the reversible electrochemical reactions occurring in the VOCl-MMC battery during cycling was possible which is shown as a sketch in Figure 5. In the initial charge process, the chloride ions dissociate from the MMC anode ($MgCl_2 + 2e^- \rightarrow Mg + 2Cl^-$) and migrate to the VOCl cathode.[20] There, an oxidation reaction occurs, resulting in the formation of $VOCl_2$ phase ($VOCl + Cl^- \rightarrow VOCl_2 + e^-$). In the following discharge, both $VOCl_2$ and the residual VOCl are partially reduced to VO and the chloride ions move back to the anode.

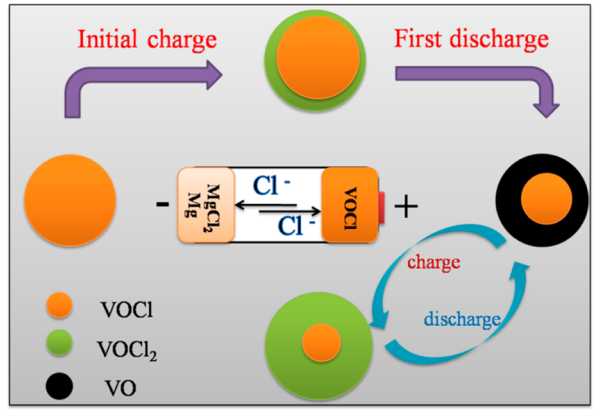

Figure 5. Schematic illustration of the phase evolution for the VOCl-MMC battery upon the charge and discharge reactions.

4. CONCLUSION

In summary, we have presented a first room temperature rechargeable chloride ion battery using VOCl/C as cathode and $MgCl_2$/Mg/C composite as anode in an ionic liquid electrolyte. The charge and discharge mechanism was characterized by XRD, XPS, and electrochemical measurements. The results revealed that the VOCl/C cathode can be charged and discharged with Mg/C or $MgCl_2$/Mg/C composite as anode. The formation of $VOCl_2$ and VO phases during cycling in the VOCl-MMC battery demonstrated that the chloride ion can be shuttled between cathode and anode. This particular setup delivered a discharge capacity of 101 mAh g^{-1} after an activation process in initial cycles and retained 60 mAh g^{-1} after 53 cycles in this first study.

■ ASSOCIATED CONTENT

Supporting Information

X-ray diffraction, EIS, XPS survey spectra, morphology of the as-prepared materials, and charge/discharge performance of cell at a current density of 5 mAh g^{-1}. This material is available free of charge via the Internet at http://pubs.acs.org.

■ AUTHOR INFORMATION

Corresponding Authors

*E-mail: m.fichtner@kit.edu. Tel.: +49 (0)721 608 25340. Fax: +49 (0)721 608 6368 (M.F.).

*E-mail: xiangyu.zhao@njtech.edu.cn (X.Z.).

Notes

The authors declare no competing financial interest.

■ ACKNOWLEDGMENTS

Financial support from China Scholarship Council (CSC) is gratefully acknowledged. X.Z. acknowledges the support from the Priority Academic Program Development of Jiangsu Higher Education Institutions (PAPD) and the project supported by the Joint Funds of the National Natural Science Foundation of China (Grant No. U1407106). The authors also wish to thank Dr. Johannes Biskupek and Prof. Ute Kaiser, both of Ulm University, for helpful discussions.

■ REFERENCES

(1) Goodenough, J. B.; Kim, Y. Challenges for Rechargeable Li Batteries. *Chem. Mater.* **2010**, *22*, 587−603.
(2) Bruce, P. G.; Freunberger, S. A.; Hardwick, L. J.; Tarascon, J. M. Li−O_2 and Li−S Batteries with High Energy Storage. *Nat. Mater.* **2012**, *11*, 19−29.
(3) Scrosati, B.; Hassoun, J.; Sun, Y.-K. Lithium-Ion Batteries. A Look into the Future. *Energy Environ. Sci.* **2011**, *4*, 3287−3295.
(4) Chevrier, V. L.; Ceder, G. Challenges for Na-Ion Negative Electrodes. *J. Electrochem. Soc.* **2011**, *158*, A1011−A1014.
(5) Slater, M. D.; Kim, D.; Lee, E.; Johnson, C. S. Sodium-Ion Batteries. *Adv. Funct. Mater.* **2013**, *23*, 947−958.
(6) Kim, S.-W.; Seo, D.-H.; Ma, X.; Ceder, G.; Kang, K. Electrode Materials for Rechargeable Sodium-Ion Batteries: Potential Alternatives to Current Lithium-Ion Batteries. *Adv. Energy Mater.* **2012**, *2*, 710−721.
(7) Aurbach, D.; Lu, Z.; Schechter, A.; Gofer, Y.; Gizbar, H.; Turgeman, R.; Cohen, Y.; Moshkovich, M.; Levi, E. Prototype Systems for Rechargeable Magnesium Batteries. *Nature* **2000**, *407*, 724−726.
(8) Zhao-Karger, Z.; Zhao, X.; Fuhr, O.; Fichtner, M. Bisamide Based Non-Nucleophilic Electrolytes for Rechargeable Magnesium Batteries. *RSC Adv.* **2013**, *3*, 16330−16335.
(9) Xu, C.; Li, B.; Du, H.; Kang, F. Energetic Zinc Ion Chemistry: The Rechargeable Zinc Ion Battery. *Angew. Chem., Int. Ed.* **2012**, *124*, 957−959.
(10) Jayaprakash, N.; Das, S. K.; Archer, L. A. The Rechargeable Aluminum-Ion Battery. *Chem. Commun.* **2011**, *47*, 12610−12612.
(11) Anji Reddy, M.; Fichtner, M. Batteries Based on Fluoride Shuttle. *J. Mater. Chem.* **2011**, *21*, 17059−17062.
(12) Gschwind, F.; Zhao-Karger, Z.; Fichtner, M. A Fluoride-Doped PEG Matrix as an Electrolyte for Anion Transportation in a Room-Temperature Fluoride Ion Battery. *J. Mater. Chem. A* **2014**, *2*, 1214−1218.
(13) Zhao, X.; Ren, S.; Bruns, M.; Fichtner, M. Chloride Ion Battery: A New Member in the Rechargeable Battery Family. *J. Power Sources* **2014**, *245*, 706−711.
(14) Zhao, X.; Zhao-Karger, Z.; Wang, D.; Fichtner, M. Metal Oxychlorides as Cathode Materials for Chloride Ion Batteries. *Angew. Chem., Int. Ed.* **2013**, *52*, 13621−13624.
(15) Schaefer, H.; Wartenpfuhl, F. Ueber das Vanadin (III) Oxydchorid VOCl. *J. Less-Common Met.* **1961**, *3*, 29−33.
(16) Glawion, S.; Scholz, M. R.; Zhang, Y.-Z.; Valenti, R.; Saha-Dasgupta, T.; Klemm, M.; Hemberger, J.; Horn, S.; Sing, M.; Claessen. Electronic Structure of the Two-Dimensional Heisenberg Antiferromagnet VOCl: A Multiorbital Mott Insulator. R. *Phys. Rev. B* **2009**, *80*, 1551191−1551196.
(17) Hryha, E.; Rutqvist, E.; Nyborg, L. Stoichiometric Vanadium Oxides Studied by XPS. *Surf. Interface Anal.* **2012**, *44*, 1022−1025.
(18) Werfel, F.; Draeger, G.; Berg, U. X-ray and X-ray Photoelectron Spectra of Vanadium Oxides. *Cryst. Res. Technol.* **1981**, *16*, 119−126.
(19) Nakai, I.; Ggawa, H.; Sugitani, Y.; Niwa, Y.; Nagashima, K. X-ray Photoelectron Spectroscopic Study of Vanadium-Bearing Aegirines. *Mineral. J.* **1976**, *8*, 129−134.
(20) Zhao, X.; Li, Q.; Zhao-Karger, Z.; Gao, P.; Fink, K.; Shen, X.; Fichtner, M. Magnesium Anode for Chloride Ion Batteries. *ACS Appl. Mater. Interfaces.* **2014**, *6*, 10997−11000.